MITSUBISHI ELECTRIC RESEARCH LABORATORIES
https://www.merl.com

Doppler Single-Photon Lidar

Kitichotkul, Ruangrawee; Rapp, Joshua; Ma, Yanting; Mansour, Hassan

TR2025-028 March 08, 2025

Abstract

Single-photon lidar (SPL) can achieve high-accuracy, low- light ranging; however, velocity estimation typically requires regression over multiple distance measurements. Here, we introduce Doppler SPL, which enables joint instantaneous velocity and range estimation. First, we derive a measurement model for SPL, showing that a target moving at a constant velocity introduces a Doppler shift into the sequence of photon detection times. We then introduce estimators for range and velocity based on Fourier analysis of the detection time sequence. Simulations show improved accuracy of our method over baseline approaches, and we further validate our approach on experimental SPL data for a moving target.

IEEE International Conference on Acoustics, Speech, and Signal Processing (ICASSP) 2025

Mitsubishi Electric Research Laboratories, Inc.
201 Broadway, Cambridge, Massachusetts 02139

Doppler Single-Photon Lidar

Ruangrawee Kitichotkul*
Boston University
Boston, MA 02215, USA
email: rkitich@bu.edu

Joshua Rapp, Yanting Ma, and Hassan Mansour
Mitsubishi Electric Research Laboratories (MERL)
Cambridge, MA 02139, USA
email: {rapp, yma, mansour}@merl.com

***Abstract*—Single-photon lidar (SPL) can achieve high-accuracy, low-light ranging; however, velocity estimation typically requires regression over multiple distance measurements. Here, we introduce Doppler SPL, which enables joint instantaneous velocity and range estimation. First, we derive a measurement model for SPL, showing that a target moving at a constant velocity introduces a Doppler shift into the sequence of photon detection times. We then introduce estimators for range and velocity based on Fourier analysis of the detection time sequence. Simulations show improved accuracy of our method over baseline approaches, and we further validate our approach on experimental SPL data for a moving target.**

***Index Terms*—Single-photon lidar, Doppler shift, velocity estimation, Fourier analysis**

I. Introduction

Lidar is a powerful technology for high-accuracy distance measurement, with a broad set of applications related to mapping, navigation, and 3D sensing. Velocity information is increasingly desired, for example in autonomous vehicle settings, where it can help distinguish moving cars and pedestrians from static backgrounds [1]–[4]. The ability to simultaneously measure range and velocity is an oft-cited advantage of coherent lidar systems over more conventional time-of-flight (ToF) lidar [5]–[7]. In frequency-modulated continuous wave (FMCW) lidar, for instance, radial velocity is encoded in the Doppler shift of the *optical frequency* and can be recovered jointly with the range measurement.

In contrast, the classical approach to velocity estimation for ToF lidar is to make two or more separate distance measurements and then use regression to compute the rate of change [8]–[12]. Unfortunately, tracking changes in distance across multiple measurement frames is challenging if targets also have lateral motion, and assuming the scene is quasi-static within an acquisition frame degrades the performance for fast-moving targets. Heide et al. [13] demonstrated that radial velocity can be measured in indirect ToF, or amplitude-modulated continuous wave (AMCW) lidar, due to the Doppler shift in the *modulation frequency*. Distance and radial velocity can be recovered by combining homodyne and heterodyne measurements [13], [14]. So far, however, there has been no equivalent approach for direct ToF, also known as pulsed lidar.

Single-photon lidar (SPL) is a type of pulsed lidar that detects photons with a single-photon-sensitive detector, such as a single-photon avalanche diode (SPAD), and time-stamps the detections with picosecond-resolution, enabling superior long-distance and low-light ranging ability compared to FMCW and AMCW [15], [16]. Unlike other pulsed lidar, which measures range from a single pulse, SPL uses a sequence of pulses to increase the probability of detecting photons. In this paper, we recognize that the periodic illumination of SPL can be considered to be a form of AMCW, where the amplitude modulation is a pulse train rather than a sinusoid. Thus, the velocity of an illuminated target likewise causes a Doppler shift, which we observe as a change in the *pulse repetition frequency*. Wei et al. [17] recently showed Fourier analysis of detection time sequences could be used for passive single-photon imaging. Inspired by [17], we show that similar analysis applied to a synchronized SPL system enables range and velocity estimation from the amplitude and phase of the detection sequence spectrum. In summary, we make the following contributions:

1) We derive an SPL measurement model for a moving target with a constant velocity.
2) We propose a method for simultaneously estimating the target's instantaneous velocity and distance based on Fourier analysis of the detection times.
3) We show that our proposed method improves the accuracy of velocimetry and ranging over baseline methods that assume quasi-static frames. We also demonstrate that the proposed method is applicable to real SPL measurements.

The accuracy of our method is invariant to velocity, whereas the quasi-static baseline methods become less accurate as the speed increases. The main limitation of our proposed method is its sensitivity to ambient light, particularly for range estimation.

*This work was completed while R. K. was an intern at MERL.

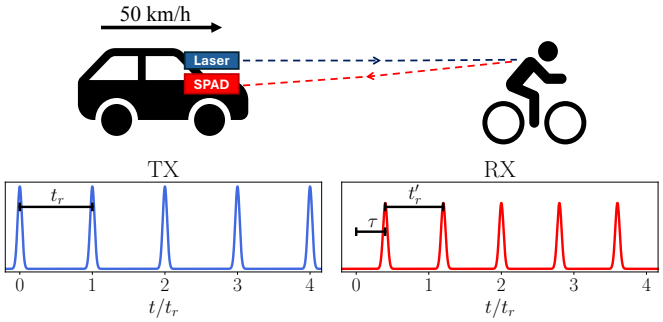

Fig. 1: A schematic portraying a moving target moving toward an SPL system with a constant relative velocity. The repetition period of the detection intensity (bottom right) is shorter than that of the transmitting signal (bottom left) due to the Doppler shift. Note the scale is exaggerated for illustration.

II. Photon Detection Model

Fig. 1 depicts a sketch of an example acquisition scenario. Suppose a laser emits n_{r} periodic pulses with repetition period t_{r} and pulse shape $h(t)$, where $\int_{-\infty}^{\infty} h(t)\mathrm{d}t = 1$. Then the intensity of the periodic illumination pulse train is given as

$$\mu(t) = \gamma \sum_{n=0}^{n_{\mathrm{r}}-1} h(t - nt_{\mathrm{r}}), \tag{1}$$

where γ is a scaling factor related to the illumination power. It is well-established that if an illuminated target is static, photon detection is an inhomogeneous Poisson process whose intensity function is

an attenuated and time-shifted version of $\mu(t)$ [18]. SPL distance estimates usually harness the statistics of detection times relative to the most recent pulse time, discarding the absolute detection sequence.

Instead, we consider that the target could be moving with constant velocity v over the acquisition interval $[0, t_\mathrm{a})$, where $t_\mathrm{a} = n_\mathrm{r} t_\mathrm{r}$. Let the starting distance of the target be z_0, so the time-of-flight in a static setting would be $\tau_0 = 2z_0/c$, where c is the speed of light. Let S denote the signal flux, i.e., the mean number of back-reflected photons detected per illumination cycle, which is proportional to γ, the target albedo, the detector efficiency, and a radial fall-off factor. Let b denote the intensity of the ambient background light. The signal-to-background ratio (SBR) is given as $S/(bt_\mathrm{r})$. Due to the motion of the target, the photon detection intensity accounting for the Doppler shift is given as

$$\lambda(t) = S\left[\sum_{n=0}^{n_\mathrm{r}-1} h\left(t - \frac{c}{c-v}\tau_0 - n\frac{c+v}{c-v}t_\mathrm{r}\right)\right] + b. \tag{2}$$

We observe that the target velocity not only affects the time-of-flight of photons after each illumination pulse but also effectively changes the periodicity of the detections. We can thus define $\tau = c\tau_0/(c-v)$ as the initial delay in the acquisition interval and $t'_\mathrm{r} = \frac{c+v}{c-v}t_\mathrm{r}$ to be the repetition period of the detection process, as shown in Fig. 1. We suppose a SPAD detects N photons over $[0, t_a)$, and we record the detection times $\mathcal{T} := (T_i)_{i=1}^N$ relative to $t = 0$. We assume that the total flux is low enough that dead-time effects are negligible.

III. Method

We propose to estimate the velocity v by exploiting the difference between the transmitting frequency $f_\mathrm{r} = 1/t_\mathrm{r}$ and the Doppler-shifted receiving frequency $f'_\mathrm{r} = 1/t'_\mathrm{r}$. The phase of the detection times will also reveal the time-of-flight τ. We first discuss spectral analysis of photon detection times and then describe the estimators for v and initial distance z_0.

A. Flux Probing

The *intensity spectrum*, i.e., the Fourier transform of the detection intensity (2), is

$$\widetilde{\lambda}(f) = Sf'_\mathrm{r}t_\mathrm{a}\sum_{k=-\infty}^{\infty}\Big\{e^{-j2\pi\left[kf'_\mathrm{r}\tau + \frac{t_\mathrm{a}}{2}(f-kf'_\mathrm{r})\right]}\widetilde{h}(kf'_\mathrm{r}) \operatorname{sinc}[t_\mathrm{a}(f-kf'_\mathrm{r})]\Big\} + bt_\mathrm{a}e^{-j\pi f t_\mathrm{a}}\operatorname{sinc}(t_\mathrm{a}f) \tag{3}$$

where $\widetilde{h}(f)$ is the Fourier transform of $h(t)$. The magnitude $|\widetilde{\lambda}(f)|$ has local maxima near the harmonics of the receiving frequency f'_r. We propose to estimate f'_r by identifying these local maxima. By applying *flux probing* to the detection times $\mathcal{T}$ [17], we form an estimate of the intensity spectrum called the *probed spectrum*:

$$\varphi_\mathcal{T}(f) := \sum_{T\in\mathcal{T}} \exp(-j2\pi fT). \tag{4}$$

Fig. 2(a) shows the magnitudes of the detection and probed spectra.

According to Wei et al. [17], $\varphi_\mathcal{T}(f)/t_\mathrm{a}$ converges in probability to $\widetilde{\lambda}(f)/t_\mathrm{a}$ as $t_\mathrm{a} \to \infty$. However, we observe significant differences between the expected and empirical spectra due to the finite acquisition interval and randomness of detection times. For instance, the background contribution to the *intensity* spectrum is negligible for frequencies greater than a few multiples of $1/t_\mathrm{a}$, which is typically much smaller than f'_r. However, we observe significant background in the *probed* spectrum even at high frequencies, as demonstrated in Figure 2(a). Our estimators, which are based on the assumption $b = 0$, are thus affected by the presence of background detections.

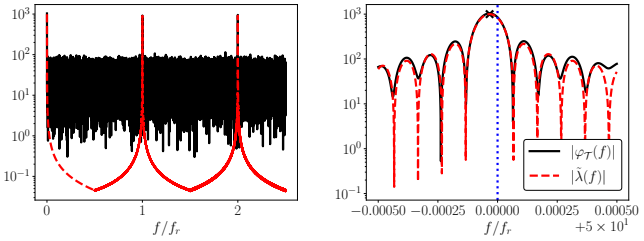

(a) DC to 2^{nd} harmonic (b) 50^{th} harmonic

Fig. 2: Magnitude of the intensity spectrum $\widetilde{\lambda}(f)$ and the probed spectrum $\varphi_\mathcal{T}(f)$ at frequencies spanning the first harmonics (a) and around the 50^{th} harmonic (b) for a target with velocity $50\,\mathrm{m/s}$. The vertical line in (b) denotes $50f_\mathrm{r}$, from which the spectrum's local maximum $50f'_\mathrm{r}$ deviates.

B. Velocimetry with Probed Spectral Magnitude

We aim to estimate the target velocity from the Doppler shift of f_r relative to f'_r. We propose a receiving frequency estimator

$$\widehat{f}'_\mathrm{r} = \operatorname*{arg\,max}_{f\in[f_\mathrm{min}, f_\mathrm{max}]} \sum_{k\in\mathcal{K}} |\varphi_\mathcal{T}(kf)|^2, \tag{5}$$

where $\mathcal{K}$ is a set of positive integers indexing the harmonics of f'_r, and f_min and f_max bound the search region. Because of the multimodal spectrum, as shown in Fig. 2(b), the optimization objective in (5) is typically nonconcave. In our implementation, we initialize the maximization with a coarse grid search in $[f_\mathrm{min}, f_\mathrm{max}]$ and then refine the peak estimate using the L-BFGS-B algorithm [19]. To determine the search range, we choose an *a priori* maximum speed v_max and compute the minimum and maximum of possible Doppler-shifted frequencies:

$$f_\mathrm{min} = \frac{c - v_\mathrm{max}}{c + v_\mathrm{max}} f_\mathrm{r}, \quad f_\mathrm{max} = \frac{c + v_\mathrm{max}}{c - v_\mathrm{max}} f_\mathrm{r}. \tag{6}$$

Given $\widehat{f}'_\mathrm{r}$, the corresponding velocity estimate is then

$$\widehat{v} = c(f_\mathrm{r} - \widehat{f}'_\mathrm{r})/(f_\mathrm{r} + \widehat{f}'_\mathrm{r}). \tag{7}$$

When $\mathcal{K} = \{1\}$, our estimator is identical to maximizing the Bartlett periodogram for Poisson processes [20], which has been proven to yield a consistent estimator for certain classes of intensity functions [21]. Because the pulse $h(t)$ is narrow, its spectrum decays slowly, and we can use a large set of harmonics $\mathcal{K} = \{1, 2, \ldots, k_\mathrm{max}\}$ to reduce the variance of the estimate $\widehat{f}'_\mathrm{r}$. The reliability of the higher harmonics is limited by the timing resolution of the SPL system, which depends on the quantization of the time-stamping electronics, time jitter, and the laser pulse width. Assuming the overall timing resolution can be approximated as a Gaussian function with scaling parameter σ, we approximate the effective resolution as $t_\mathrm{res} \approx 4\sigma$. We then ensure the highest probe frequency $k_\mathrm{max} f_\mathrm{max}$ does not exceed the Nyquist rate $f_\mathrm{Nyquist} = 1/(2t_\mathrm{res})$ [17].

C. Ranging with Probed Spectral Phase

The phase of the probed spectrum reveals the target's distance. Suppose that $b = 0$, and assume $h(t)$ is real and even. Then, the phase of the intensity spectrum (3) at the receiving frequency f'_r is dominated by the $k = 1$ term:

$$\arg\left[\widetilde{\lambda}(f'_\mathrm{r})\right] \approx (-2\pi f'_\mathrm{r}\tau) \bmod 2\pi. \tag{8}$$

By replacing $\arg[\widetilde{\lambda}(f_{\mathrm{r}}')]$ with the *probed phase* $\arg[\varphi_{\mathcal{T}}(f)]$ at the estimated receiving repetition frequency $\widehat{f}_{\mathrm{r}}'$ computed with (5) and using $\widehat{t}_{\mathrm{r}}' := 1/\widehat{f}_{\mathrm{r}}'$, we can estimate the pulse return time as

$$\widehat{\tau} = \left\{ -\widehat{t}_{\mathrm{r}}' \arg\left[\varphi_{\mathcal{T}}(\widehat{f}_{\mathrm{r}}')\right]/(2\pi) \right\} \bmod \widehat{t}_{\mathrm{r}}'. \tag{9}$$

Assuming the modulo has not caused aliasing [22], estimates $\widehat{\tau}_0$ and $\widehat{z}_0$ can be computed through the relations $\tau_0 = (c - v)\tau/c$ and $z_0 = c\tau_0/2$. Note that this estimator ignores the effect of background, which also contributes to the phase.

D. Baseline Methods

Previous methods estimate the velocity and distance of a moving target by regressing estimated distances over multiple time frames [8]–[12]. While there are variations in how the frames are processed, they all rely on the common assumption that dynamic scenes can be considered quasi-static over short time frames [23]–[28].

Following previous works, our baseline method divides the acquisition time into subframes and applies linear regression to the estimated distances. We take the slope as the velocity estimate, and the intercept as the initial distance estimate. Suppose the acquisition time $[0, t_{\mathrm{a}})$ is divided into F equal subframes $\left\{\left[\frac{\ell-1}{F}t_{\mathrm{a}}, \frac{\ell}{F}t_{\mathrm{a}}\right)\right\}_{\ell=1}^{F}$. Let $\widehat{z}_\ell$ denote a distance estimate from a quasi-static estimator using only the detection times within the ℓ^{th} subframe $\mathcal{T}_\ell$. We associate $\widehat{z}_\ell$ with the center of the ℓ^{th} subframe $t_\ell = t_{\mathrm{a}}(\ell - 1/2)/F$ for any $\ell \in \{1, \ldots, F\}$. The baseline method estimates the velocity and initial distance using linear regression:

$$\widehat{v}, \widehat{z}_0 = \underset{v, z_0}{\arg\min} \sum_{\ell=1}^{F} \left[(z_0 + v t_\ell) - \widehat{z}_\ell\right]^2. \tag{10}$$

In this paper, we use two quasi-static distance estimators. The first is a log-matched filter:

$$\widehat{z}_\ell = \underset{z}{\arg\max} \sum_{T \in \mathcal{T}_\ell} \log h\left(T_\ell \bmod t_{\mathrm{r}} - \frac{2z}{c}\right), \tag{11}$$

which is the maximum likelihood (ML) estimator of the distance when $b = 0$ and the target is static [18]. The second is the ML estimator when $b > 0$:

$$\widehat{z}_\ell = \underset{z, S, b}{\arg\max} \sum_{T \in \mathcal{T}_\ell} \log\left[Sh\left(T_\ell \bmod t_{\mathrm{r}} - \frac{2z}{c}\right) + b\right]. \tag{12}$$

Even though the optimization objective is nonconcave, the estimate can be computed efficiently by using alternating maximization [29].

IV. Experiments

A. Simulation Results

For all simulations, we set $t_{\mathrm{r}} = 1\,\mu\mathrm{s}$ and $n_{\mathrm{r}} = 10^4$. The pulse shape is Gaussian with width $\sigma = 100\,\mathrm{ps}$. The Nyquist rate for the proposed method, limited by the pulse width, is $f_{\mathrm{Nyquist}} = 2.5\,\mathrm{GHz}$. To determine the search region for the proposed method as described in (6), we assume that the target does not move faster than $v_{\max} = 150\,\mathrm{m/s}$. Although $k_{\max}$ could be as high as 1249, we set $k_{\max} = 200$ to reduce the computation time.

1) No Ambient Light: We simulate detection times from SPL for a moving target based on the intensity function (2) and compute estimates of the velocity v and initial distance z_0 using the proposed and baseline methods. We compute the root mean square error (RMSE) of each estimator for a given simulation setting from 1000 Monte Carlo trials. We first demonstrate that the proposed estimators (5) and (9) improve velocimetry and ranging over the baseline when there is no ambient light, i.e., $b = 0$. The target velocity ranges from -50 to $50\,\mathrm{m/s}$, and we set $S = 0.1$. Since $b = 0$, we use the log-matched filter (11) for the baseline method. As shown in Fig. 3, the proposed method yields more accurate velocity and distance estimates than the baseline method at any velocity and is equally accurate at any velocity. The accuracy of the baseline method improves by increasing the number of subframes, but the baseline performance still degrades as the speed increases due to the quasi-static assumption.

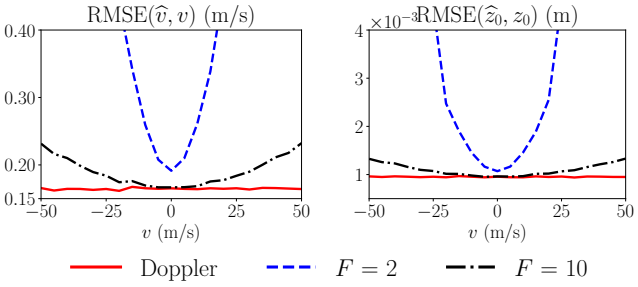

Fig. 3: RMSE of velocity and distance estimates when $b = 0$. *Doppler* denotes the proposed method. The baseline method uses (11) with 2 or 10 subframes.

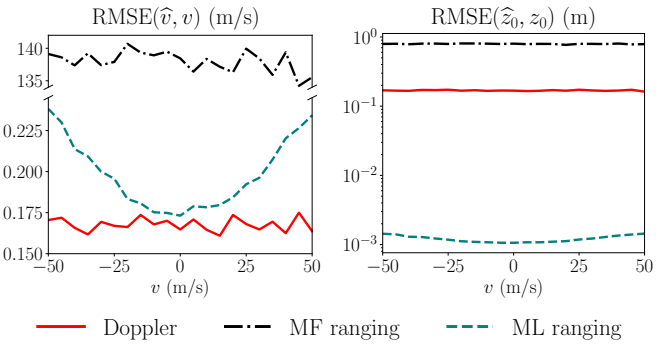

Fig. 4: RMSE of velocity and distance estimates when SBR = 10. *Doppler* denotes the proposed method. *MF ranging* uses (11), and *ML ranging* uses (12); both baseline methods use 10 subframes.

2) Low Ambient Light: Next, we evaluate the estimators when there is ambient light. The simulation settings are the same as those described above but now with $b = 10^4\,\mathrm{counts/s}$, corresponding to SBR $= 10$. We also compare the two baseline distance estimators—the log-matched filter (11) and the ML estimator (12)—using $F = 10$ subframes. As shown in Fig. 4, the proposed velocity estimator yields lower RMSE than the baseline methods and remains equally accurate at any velocity in presence of ambient light, though its RMSE slightly increases from when $b = 0$. The baseline velocity estimator with ML ranging achieves slightly higher RMSE than the proposed method at $v = 0\,\mathrm{m/s}$, and the error again increases with the target's speed. The baseline with log-matched filter completely fails in presence of ambient light. While ambient light slightly increases the RMSE of the proposed velocity estimator, it increases the RMSE of the proposed distance estimator by 2 orders of magnitude. This result is not surprising, since the background level changes the phase of the intensity spectrum (3). On the contrary, the baseline with ML ranging, which implicitly censors the background detections [29], has similar RMSE as when $b = 0$.

3) Imaging Example: We simulate SPL measurements of a 3D scene with three moving targets in front of a static background when $b = 0$ (SBR $= \infty$) and $b = 1.63 \times 10^3\,\mathrm{counts/s}$, corresponding to an

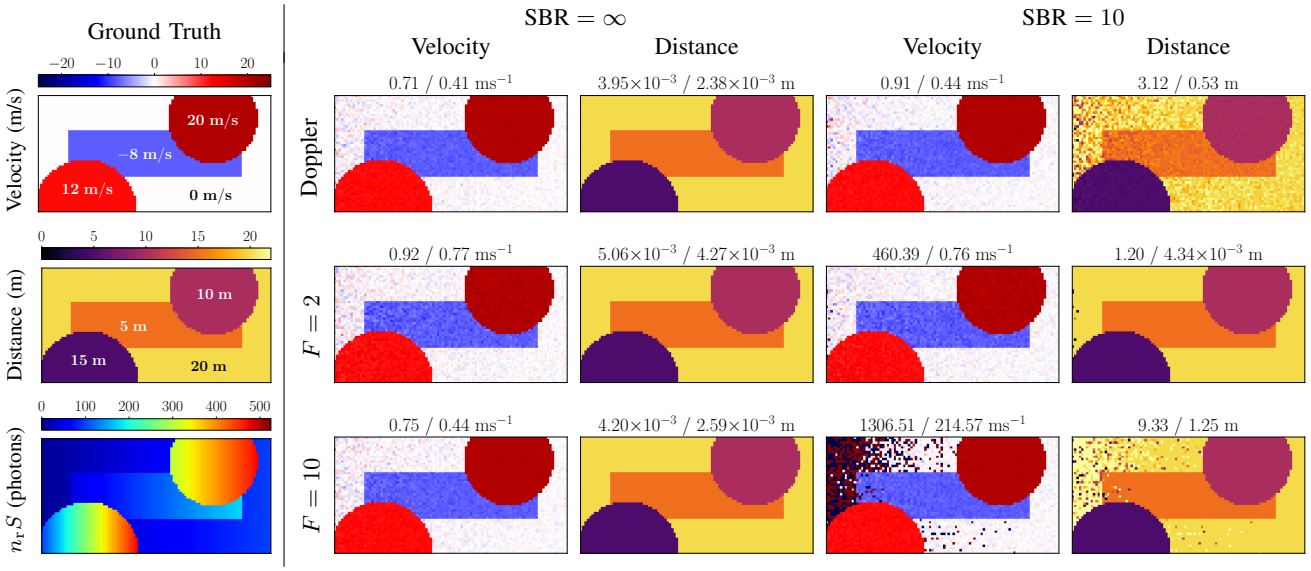

Fig. 5: Velocimetry and ranging of a simulated 3D scene with three moving targets. *Doppler* denotes the proposed method, while $F = 2$ and $F = 10$ denote the baseline methods with 2 and 10 subframes using (11) when SBR $= \infty$ and (12) when SBR $= 10$. The mean number of signal photons $n_r S$ increases from left to right, as shown in the bottom left plot. The pixels on the targets have higher $n_r S$ than those on the static background. The numbers above each estimate plot are the RMSE for all pixels (before /) and for only the moving targets (after /).

average SBR of 10. We design the signal flux in the scene to increase from left to right to demonstrate the effect of varying number of signal detections. The ground truth and the estimates are shown in Fig. 5 and confirm our observations from the numerical evaluations. When SBR $= \infty$, the proposed method yields more accurate estimates of both velocity and distance than the baseline methods. At SBR $= 10$, our proposed velocity estimates are fairly robust to the background detections and still outperform the baseline methods, whereas our distance estimates incur significant error. As expected, the accuracy increases with the number of photon detections.

At SBR $= \infty$, increasing the number of frames reduces the RMSE of the baseline estimator. However, when SBR $= 10$, the baseline method with $F = 10$ yields higher RMSE than with $F = 2$ due to many erroneous pixels with low $n_r S$ on the left-hand side of the image. This result demonstrates a weakness of the baseline method: using more subframes reduces high-velocity errors, but dividing the acquisition into too many subframes may result in insufficient numbers of signal photons in some subframes, leading to distance—and ultimately velocity—estimation errors. In contrast, our proposed method uses the full detection sequence without dividing into subframes, and the accuracy is not velocity-dependent.

B. Experimental Results

We further validate our approach on real SPL measurements. Our experimental setup consists of a pulsed laser at 450 nm with repetition frequency $f_r = 25$ MHz and pulse width $\sigma = 97$ ps, corresponding to the Nyquist rate $f_{\text{Nyquist}} = 2.58$ GHz and the highest allowed harmonics $k_{\max} = 51$. The target is a white card fixed to a 3 m linear translation stage controlled by a stepper motor. A draw-wire linear encoder is synchronized to the time-tagging module to provide a reference distance measurement of the moving target. We take the differential velocity from adjacent distance readings as the reference velocity. The detection times are grouped into frames of duration 25 ms, corresponding to a 40 frames/s acquisition, and we estimate the distance and velocity for each frame. The result

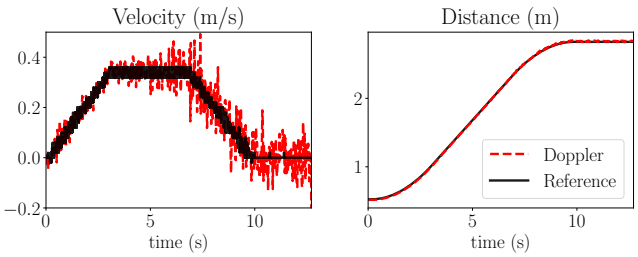

Fig. 6: Estimated velocity and distance using the proposed method with real SPL measurements. The number of photon detections, and thus the accuracy, decreases as the distance increases.

is shown in Fig. 6. Our velocity and distance estimates track the reference measurements from the linear encoder well. We remark that the velocity estimates become less accurate as the target moves farther away, because fewer photons are reflected back to the SPAD due to the distance fall-off. The estimated SBR during the acquisition decreases from 15 to 7 as the target moves away from the detector.

V. Conclusion

We derive a photon detection model for SPL when the target is moving at a constant velocity. We propose a velocity estimator that quantifies the Doppler shift due to movement and an initial distance estimator based on the phase of the detection times. Our method enables simultaneous velocity and range measurements that remain accurate even for fast moving targets. Some future directions include improving the robustness of the estimators against ambient light, incorporating velocity estimation in tracking algorithms for SPL measurements, and modeling the target's acceleration and higher-order derivatives of position.

References

[1] Z. Lin, M. Hashimoto, K. Takigawa, and K. Takahashi, "Vehicle and pedestrian recognition using multilayer lidar based on support vector

machine," in *Int. Conf. Mechatron. Mach. Vis. Pract. (M2VIP)*, 2018, pp. 1–6.

[2] X. Peng and J. Shan, "Detection and tracking of pedestrians using Doppler lidar," *Remote Sens.*, vol. 13, no. 15, Art. no. 2952, 2021.

[3] Y. Jin, Y. Kuang, M. Hoffmann, C. Schüßler, A. Deligiannis, J.-C. Fuentes-Michel, and M. Vossiek, "Radar and lidar deep fusion: Providing Doppler contexts to time-of-flight lidar," *IEEE Sensors J.*, vol. 23, no. 20, pp. 25587–25600, 2023.

[4] L. Alexandrino, H. Z. Olyaei, A. Albuquerque, P. Georgieva, and M. V. Drummond, "3D object detection for self-driving vehicles enhanced by object velocity," *IEEE Access*, vol. 12, pp. 8220–8229, 2024.

[5] J. Riemensberger, A. Lukashchuk, M. Karpov, W. Weng, E. Lucas, J. Liu, and T. J. Kippenberg, "Massively parallel coherent laser ranging using a soliton microcomb," *Nature*, vol. 581, no. 7807, pp. 164–170, May 2020.

[6] H. Jang, J. W. Kim, G. H. Kim, C. H. Park, S. W. Jun, M. Jo, H. Lee, and C.-S. Kim, "Simultaneous distance and vibration mapping of FMCW-LiDAR with akinetic external cavity diode laser," *Opt. Lasers Eng.*, vol. 160, Art. no. 107283, Jan. 2023.

[7] P. Mirdehghan, B. Buscaino, M. Wu, D. Charlton, M. E. Mousa-Pasandi, K. N. Kutulakos, and D. B. Lindell, "Coherent optical modems for full-wavefield lidar," June 2024, arXiv:2406.08439 [physics].

[8] P. Jonsson, J. Hedborg, M. Henriksson, and L. Sjöqvist, "Reconstruction of time-correlated single-photon counting range profiles of moving objects," in *Proc. SPIE Electro-Opt. Remote Sens. Photon. Tech. Appl. IX*, 2015, vol. 9649, pp. 11–18.

[9] J. Hedborg, P. Jonsson, M. Henriksson, and L. Sjöqvist, "Time-correlated single-photon counting range profiling of moving objects," in *Int. Laser Radar Conf.*, 2016, vol. 119 of *EPJ Web of Conferences*, Art. no. 06010.

[10] W. Xue, L. Liu, X. Dai, and Y. Luo, "Moving target ranging method for a photon-counting system," *Opt. Express*, vol. 26, no. 26, pp. 34161–34178, Dec. 2018.

[11] A. Hou, Y. Hu, Y. Xie, N. Zhao, S. Xu, Y. Wang, X. Zhang, F. Han, and J. Fang, "Full waveform recovery method of moving target for photon counting lidar," *IEEE Trans. Geosci. Remote Sensing*, vol. 62, pp. 1–14, 2024.

[12] X. Liu, J. Qiang, G. Huang, L. Zhang, Z. Zhao, and R. Shu, "Velocity-based sparse photon clustering for space debris ranging by single-photon lidar," arXiv:2401.04147 [physics.data-an], 2024.

[13] F. Heide, W. Heidrich, M. Hullin, and G. Wetzstein, "Doppler time-of-flight imaging," *ACM Trans. Graph.*, vol. 34, no. 4, Art. no. 36, pp. 1–11, July 2015.

[14] Y. Hu, L. Miyashita, and M. Ishikawa, "Differential frequency heterodyne time-of-flight imaging for instantaneous depth and velocity estimation," *ACM Trans. Graph.*, vol. 42, no. 1, Art. no. 9, pp. 1–13, Sept. 2022.

[15] B. Behroozpour, P. A. Sandborn, M. C. Wu, and B. E. Boser, "Lidar system architectures and circuits," *IEEE Comm. Mag.*, vol. 55, no. 10, pp. 135–142, Oct. 2017.

[16] J. Rapp, J. Tachella, Y. Altmann, S. McLaughlin, and V. K. Goyal, "Advances in single-photon lidar for autonomous vehicles: Working principles, challenges, and recent advances," *IEEE Signal Process. Mag.*, vol. 37, no. 4, pp. 62–71, 2020.

[17] M. Wei, S. Nousias, R. Gulve, D. B. Lindell, and K. N. Kutulakos, "Passive ultra-wideband single-photon imaging," in *Proc. IEEE/CVF Int. Conf. Comput. Vis.*, Paris, France, Oct. 2023, pp. 8101–8112.

[18] D. Shin, A. Kirmani, V. K. Goyal, and J. H. Shapiro, "Photon-efficient computational 3-D and reflectivity imaging with single-photon detectors," *IEEE Trans. Comput. Imaging*, vol. 1, no. 2, pp. 112–125, 2015.

[19] R. H. Byrd, P. Lu, J. Nocedal, and C. Zhu, "A limited memory algorithm for bound constrained optimization," *SIAM J. Sci. Comput.*, vol. 16, no. 5, pp. 1190–1208, Sept. 1995.

[20] M. S. Bartlett, "The spectral analysis of point processes," *J. R. Stat. Soc. B*, vol. 25, no. 2, pp. 264–281, 1963.

[21] D. Vere-Jones, "On the estimation of frequency in point-process data," *J. Appl. Probab.*, vol. 19, no. A, pp. 383–394, 1982.

[22] S. Fernandez-Menduina, J. Rapp, H. Mansour, M. Greiff, and K. Parsons, "Tracking beyond the unambiguous range with modulo single-photon lidar," in *Proc. IEEE Int. Conf. Acoust., Speech, and Signal Process.*, Apr. 2024, pp. 6–10.

[23] D. B. Lindell, M. O'Toole, and G. Wetzstein, "Single-photon 3D imaging with deep sensor fusion," *ACM Trans. Graph.*, vol. 37, no. 4, Art. no. 113, 2018.

[24] J. Tachella, Y. Altmann, N. Mellado, A. McCarthy, R. Tobin, G. S. Buller, J.-Y. Tourneret, and S. McLaughlin, "Real-time 3D reconstruction from single-photon lidar data using plug-and-play point cloud denoisers," *Nature Commun.*, vol. 10, Art. no. 4984, 2019.

[25] A. Maccarone, F. M. D. Rocca, A. McCarthy, R. Henderson, and G. S. Buller, "Three-dimensional imaging of stationary and moving targets in turbid underwater environments using a single-photon detector array," *Opt. Express*, vol. 27, no. 20, pp. 28437–28456, Sept. 2019.

[26] I. Gyongy, S. W. Hutchings, A. Halimi, M. Tyler, S. Chan, F. Zhu, S. McLaughlin, R. K. Henderson, and J. Leach, "High-speed 3D sensing via hybrid-mode imaging and guided upsampling," *Optica*, vol. 7, no. 10, pp. 1253–1260, Aug. 2020.

[27] R. Tobin, A. Halimi, A. McCarthy, P. J. Soan, and G. S. Buller, "Robust real-time 3D imaging of moving scenes through atmospheric obscurant using single-photon LiDAR," *Sci. Rep.*, vol. 11, Art. no. 11236, May 2021.

[28] S. Plosz, A. Maccarone, S. McLaughlin, G. S. Buller, and A. Halimi, "Real-time reconstruction of 3D videos from single-photon LiDaR data in the presence of obscurants," *IEEE Trans. Comput. Imaging*, vol. 9, pp. 106–119, 2023.

[29] R. Kitichotkul, J. Rapp, and V. K. Goyal, "The role of detection times in reflectivity estimation with single-photon lidar," *IEEE J. Sel. Topics Quantum Electron.*, vol. 30, no. 1, Art. no. 8800114, Jan. 2024.